Influence of dispersion in myosin filament orientation and anisotropic filament contractions in smooth muscle

Martin Kroon

www.elsevier.com/locate/yjtbi

Influence of dispersion in myosin filament orientation and anisotropic filament contractions in smooth muscle

Martin Kroon

PII: S0022-5193(10)00632-6
DOI: doi:10.1016/j.jtbi.2010.11.037
Reference: YJTBI 6259

To appear in: *Journal of Theoretical Biology*

Received date: 4 September 2010
Revised date: 6 November 2010
Accepted date: 28 November 2010

Cite this article as: Martin Kroon, Influence of dispersion in myosin filament orientation and anisotropic filament contractions in smooth muscle, *Journal of Theoretical Biology*, doi:10.1016/j.jtbi.2010.11.037

Influence of Dispersion in Myosin Filament Orientation and Anisotropic Filament Contractions in Smooth Muscle

Martin Kroon

Department of Solid Mechanics, Royal Institute of Technology, Osquars backe 1, 100 44, Stockholm

Abstract

A new constitutive model for the biomechanical behaviour of smooth muscle tissue is proposed. The active muscle contraction is accomplished by the relative sliding between actin and myosin filaments, comprising contractile units in the smooth muscle cells. The orientation of the myosin filaments, and thereby the contractile units, are taken to exhibit a statistical dispersion around a preferred direction. The number of activated cross-bridges between the actin and myosin filaments governs the contractile force generated by the muscle and also the contraction speed. A strain-energy function is used to describe the mechanical behaviour of the smooth muscle tissue. Besides the active contractile apparatus, the mechanical model also incorporates a passive elastic part. The constitutive model was compared to histological and isometric tensile test results for smooth muscle tissue from swine carotid artery. In order to be able to predict the active stress at different muscle lengths, a filament dispersion significantly larger than the one observed

Email address: martin@hallf.kth.se ()

experimentally was required. Furthermore, a comparison of the predicted active stress for a case of uniaxially oriented myosin filaments and a case of filaments with a dispersion based on the experimental histological data shows that the difference in generated stress is noticeable but limited. Thus, the results suggest that myosin filament dispersion alone cannot explain the increase in active muscle stress with increasing muscle stretch.

Keywords:
biomechanics, soft biological tissue, smooth muscle, myosin, statistical dispersion

1. Introduction

Muscle tissue is an important component in several parts of the human body and appears in three different forms: skeletal muscle, cardiac muscle, and smooth muscle. Smooth muscle tissue is found in organs such as the stomach, the intestines, the urinary bladder, the airways, and blood vessels. In the intestines, for example, the function of the muscle component is to mix and propel intraluminal contents to enable efficient digestion of food, progressive absorption of nutrients, and evacuation of residues. In vascular tissue, smooth muscle in the arterial wall regulates the diameter of the vessel and thereby the blood flow. In contrast to skeletal muscle, smooth muscle tissue contracts without conscious control. The ability to maintain prolonged contractions without showing fatigue is a property of smooth muscle that sets it apart from skeletal and cardiac muscle (Morgan et al., 1989). The reason is that the energetics of smooth muscle working at constant length is characterized by low energy consumption, ranging from 100 to 500-fold less

than skeletal muscle (Brophy, 2000; Paul, 1990; Walker et al., 1994). Smooth muscle is able to develop the same isometric force per cross-sectional area as skeletal muscle, but smooth muscle contractions are far slower (Bitar, 2003). In fact, smooth muscle shortens one to two orders of magnitude more slowly than skeletal muscle (Walker et al., 1994). Abnormal contractility of smooth muscle is an important cause of many diseases, such as hypertension and asthma (Hai and Kim, 2005). It is therefore of great interest to understand the biomechanics of smooth muscle contraction.

The physiology of smooth muscle contraction is a complex interaction between electrical, biochemical and mechanical processes. Smooth muscle is normally organized in thin layers or sheets made up of spindle-shaped cells with a single nuclei, see Fig. 1. In general, smooth muscle cells are about 200-300μm in length and 5-15μm wide (Bitar, 2003). The contractile apparatus in smooth muscle cells consists mainly of thick filaments (myosin) and thin filaments (actin). Another important component in the structure of smooth muscle cells is the cytoskeletal domain, which contains non-muscle actin and intermediate filaments. The contractile and cytoskeletal domains are connected at two other domains: the focal contact points on the membrane, dense plaques, and the focal contact points inside the cell, dense bodies. These are the points where the contractile and cytoskeletal domains connect. In vascular smooth muscle, thin filaments are far more numerous than thick filaments, giving a thin-to-thick ratio of 15:1. The average length of the thick filament in vascular smooth muscle is about 2.2μm (Fung, 1993), which is larger than for a skeletal muscle.

It appears that the myosin/actin complexes in the contractile apparatus

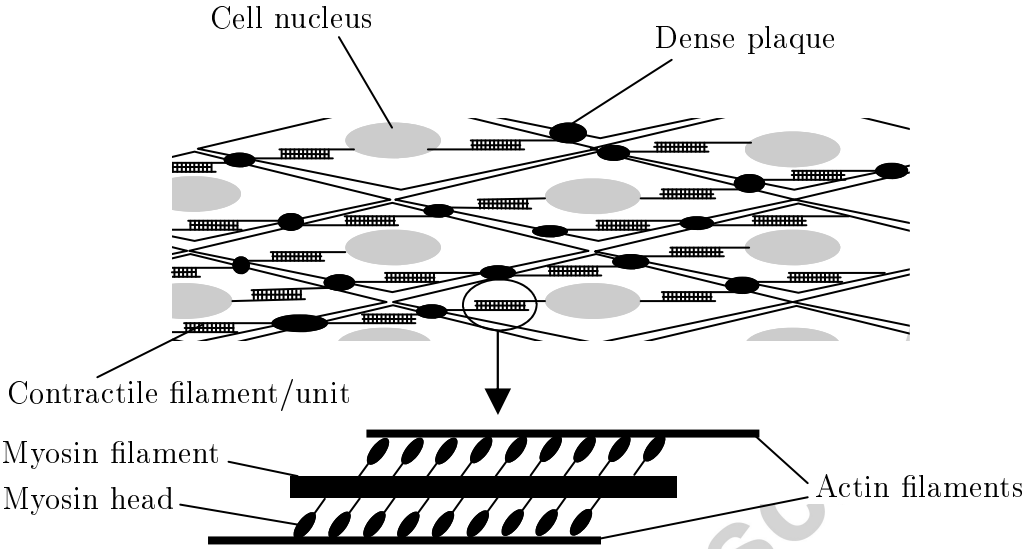

Figure 1: Structure of smooth muscle cells and a close up of a contractile filament/unit composed of a myosin (thick) filament surrounded by actin (thin) filaments. Cross-bridges (myosin heads) connect the two filament types. (From Kroon (2010a).)

have a preferred direction, coinciding with the long axis of the cell (Bitar, 2003; Herrera et al., 2005; Hodgkinson et al., 1995; Kuo and Seow, 2004; Seow and Par, 2007). Some dispersion around this direction does, however, exist (Walmsley and Murphy, 1987). Like striated muscle, smooth muscle is composed of numerous contractile units arranged in series and in parallel. The structural details of smooth muscle cells make this type of muscle compatible with a side polar model of the acto-myosin interaction and with the sliding filament mechanism of muscle contraction (Herrera et al., 2005; Hodgkinson et al., 1995). According to the sliding filament theory (Hux-

ley, 1953; Huxley and Niedergerke, 1954; Huxley and Hanson, 1954; Huxley, 1957), force is produced by cycling cross-bridges that extend from the myosin to the actin filaments. Furthermore, the side polar model implies that actin filaments on opposite sides of a myosin filament slide in opposite directions relative to each other.

The ability of smooth muscle to generate force over a large range of lengths – if given enough time to adjust – suggests that the structure of contractile units in smooth muscle is time-dependent rather than static (Bai et al., 2004; Seow and Par, 2007). This would imply that a continuous restructuring of the internal contractile apparatus and cytoskeleton takes place in the smooth muscle cells in response to the external load and the deformation imposed on the cells.

Contraction of smooth muscle cells can be initiated by mechanical, electrical, and chemical stimuli, but all of these pathways lead to an increase in intracellular Ca^{2+} concentration. An increase in intracellular free $[Ca^{2+}]$ triggers Ca^{2+} binding to calmodulin. The calcium/calmodulin complex binds to and thereby activates myosin light chain kinase (MLCK). The MLCK then in turn must activate each myosin head independently. Activation of myosin heads triggers cycling of myosin cross-bridges along the actin filaments, which induces force development or shortening of the contractile units and thereby of the muscle cell (Bitar, 2003).

Several experimental investigations on different types of smooth muscle from animals have been performed, for example smooth muscle from guinea pig taenia coli (Arner, 1982; Löfgren et al., 2001; Peterson, 1982), porcine carotid artery (Hai and Murphy, 1989; Kamm et al., 1989; Rembold and

Murphy, 1990a; Roy et al., 2005; Silver et al., 2003), porcine coronary artery (Makujina et al., 1995), porcine tracheal (Herrera et al., 2005), canine carotid artery (Takamizawa and Hayashi, 1987), ferret aorta (Jiang and Morgan, 1989), bovine tracheal (Tang et al., 1992), rat aorta (Tosun et al., 1997), and rat pulmonary artery (McIntyre Jr. et al., 1996). Several theoretical approaches, aiming at modelling different parts of the electrical-biochemical-mechanical chain in smooth muscle activation, have also been proposed (Fay and Delise, 1973; Gestrelius and Borgström, 1986; Herrera et al., 2005; Lee and Schmid-Schönbein, 1996a,b; Miftakhov and Abdusheva, 1996; Rachev and Hayashi, 1999; Rosenbluth, 1965; Stålhand et al., 2008; Yang et al., 2003a,b; Zulliger et al., 2004).

In the present paper, a theoretical model for the constitutive behaviour of smooth muscle tissue, undergoing large deformations, is proposed. The approach is based on a previous model (Kroon, 2010a), which has now been expanded to include a statistical dispersion of the orientation of myosin filaments in space. The model accounts for the calcium-activated response of smooth muscle as well as the passive response. The active response is governed by the apparatus of contractile (acto-myosin) units. These are taken to have a preferred direction but to exhibit a statistical dispersion. The influence of this statistical dispersion is the main subject of the present paper. In Sections 2 and 3, the chemical and mechanical parts of the proposed model are presented. The model is assessed using uniaxial tensile test results, and a uniaxial formulation of the model is derived in Section 4. The model is then calibrated and assessed in Section 5 using experimental results for smooth muscle from swine carotid arteries. In Section 6, the results are discussed

and summarised.

2. Chemical model

According to the sliding filament theory (Huxley, 1953; Huxley and Niedergerke, 1954; Huxley and Hanson, 1954; Huxley, 1957), muscle contraction is caused by the relative sliding of myosin and actin filaments within the muscle cells. As discussed in the previous section, the myosin and actin filaments are connected by cross-bridges, and the relative sliding between the filaments is caused by cycling of these cross-bridges, see Fig. 1. This cycling implies that cross-bridges repeatedly attach and detach. During this process, they perform a so-called power-stroke (a peddling-like movement), by which a relative sliding between the myosin and actin filaments is accomplished. In the present work, Hai and Murphy's four-state model (Hai and Murphy, 1988) is adopted, in which a cross-bridge may exist in one of four states, denoted s_1, s_2, s_3, s_4, see Fig. 2. In state s_1, the cross-bridge is passive and unable to attach to the actin filament. The MLCK enables phosphorylation of the myosin head, implying that an ATP molecule is attached to the myosin head (state s_2). In state s_2, the myosin head/cross-bridge is ready to attach to the actin filament but has not yet done so. As the cross-bridge attaches to a binding site on the actin filament, it goes to state s_3. The cross-bridge may then cycle between states s_2 and s_3, and during this cycling process, the cross-bridge performs the power-stroke. Some myosin heads may also go to a dephosphorylated state, s_4. In this state, the cross-bridge remains attached to the actin filament but does not cycle any more. The cross-bridge still generates a passive resisting force, but does not actively contribute to relative

filament sliding. Thus, states s_3 and s_4 are the only states that generate force between the filaments.

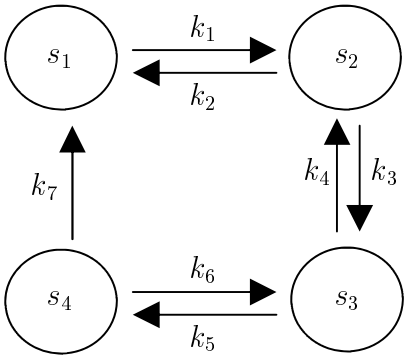

Figure 2: Four-state chemical model for cross-bridges between myosin and actin filaments proposed by Hai and Murphy (1988).

It is assumed, that a myosin filament has a total number of m_{tot} myosin heads that may potentially bind to an actin filament, and m_i denotes the number of myosin heads that, at a particular time, exist in state s_i. The fraction of the total number of myosin heads that exists in state s_i is then expressed as $n_i = m_i/m_{\text{tot}}$, where n_i are used as state variables in the chemical model. The transition of cross-bridges between the different states is taken to follow a system of linear equations:

$$\frac{\mathrm{d}\mathbf{n}}{\mathrm{d}t} = \begin{bmatrix} -k_1 & k_2 & 0 & k_7 \\ k_1 & -k_2 - k_3 & k_4 & 0 \\ 0 & k_3 & -k_4 - k_5 & k_6 \\ 0 & 0 & k_5 & -k_6 - k_7 \end{bmatrix} \mathbf{n} = \mathbf{K}\mathbf{n}. \qquad (1)$$

The vector $\mathbf{n} = (n_1 \quad n_2 \quad n_3 \quad n_4)^{\mathrm{T}}$ holds the four state variables, and the parameters $k_1, \ldots, k_7$ are rate constants, describing the rate of transition between the different states. The rate constants are contained in the system matrix $\mathbf{K}$. The state variables n_1-n_4 change according to the conservation law $n_1 + n_2 + n_3 + n_4 = 1$. Smooth muscle contraction is triggered by an increase in cytosolic $[\mathrm{Ca}^{2+}]$, and k_1 and k_6 depend directly on $[\mathrm{Ca}^{2+}]$.

3. Mechanical model

3.1. Prerequisites

The constitutive behaviour of smooth muscle tissue can be decomposed into an active and a passive part. The active part derives from the contraction of myosin/actin units in the muscle cells. The passive part is associated with the rest of the smooth muscle cells (cell membrane, cytosol, passive networks of actin, intermediate filaments, cell nuclei) and with extracellular components, such as elastin and collagen.

The constitutive behaviour of the smooth muscle is described by use of a strain-energy function Ψ, which is split into an active and a passive part Ψ_{a} and Ψ_{p}, respectively:

$$\Psi = \Psi_{\mathrm{a}} + \Psi_{\mathrm{p}} - (p_{\mathrm{a}} + p_{\mathrm{p}})(J - 1). \tag{2}$$

Two Lagrangian multipliers p_{a} and p_{p} have also been introduced to model incompressibility.

A set of basis vectors $\mathbf{e}_1$, $\mathbf{e}_2$, $\mathbf{e}_3$, defining a Cartesian coordinate system, is introduced. The position vector in the reference configuration Ω_0 and in the current configuration Ω is denoted $\mathbf{X} = X_i \mathbf{e}_i$ and $\mathbf{x} = x_i \mathbf{e}_i$, respectively.

The deformation gradient is defined as $\mathbf{F} = \partial\mathbf{x}/\partial\mathbf{X}$ ($J = \det\mathbf{F}$), and the associated right Cauchy-Green deformation tensor as $\mathbf{C} = \mathbf{F}^{\mathrm{T}}\mathbf{F}$.

The second Piola-Kirchhoff stress $\mathbf{S}$ is defined as

$$\mathbf{S} = 2\frac{\partial\Psi}{\partial\mathbf{C}} = 2\frac{\partial(\Psi_{\mathrm{a}} - p_{\mathrm{a}}(J-1))}{\partial\mathbf{C}} + 2\frac{\partial(\Psi_{\mathrm{p}} - p_{\mathrm{p}}(J-1))}{\partial\mathbf{C}} = \mathbf{S}_{\mathrm{a}} + \mathbf{S}_{\mathrm{p}}, \qquad (3)$$

where $\mathbf{S}_{\mathrm{a}}$ and $\mathbf{S}_{\mathrm{p}}$ are the contributions from the active and passive parts, respectively. From this, the first Piola-Kirchhoff stress $\mathbf{P}$ is obtained as

$$\mathbf{P} = \mathbf{F}\mathbf{S} = \mathbf{F}(\mathbf{S}_{\mathrm{a}} + \mathbf{S}_{\mathrm{p}}) = \mathbf{P}_{\mathrm{a}} + \mathbf{P}_{\mathrm{p}}. \qquad (4)$$

3.2. Constitutive behaviour for contractile apparatus

The active behaviour of smooth muscle is governed by an apparatus of contractile filaments, as illustrated in Fig. 1. These contractile filaments exist in series and in parallel inside the smooth muscle cells, and they also align with each other across cell boundaries. Smooth muscle tissues tend to have a main direction in which they contract (Bitar, 2003; Herrera et al., 2005; Hodgkinson et al., 1995; Kuo and Seow, 2004; Seow and Par, 2007). The orientation of these series of contractile filaments can therefore be described by a statistical distribution with a preferred (average) direction and an associated dispersion.

Based on the considerations above, a mechanical model for the active contractile apparatus in smooth muscle is proposed where the constitutive behaviour of this apparatus is modelled by use of a representative micro-sphere, illustrated in Fig. 3. This micro-sphere has a radius R_{rms} and includes series of contractile filaments (myosin/actin units). The orientation of a filament series is defined by a unit vector $\mathbf{M}$ ($|\mathbf{M}| = 1$), defined in the

reference configuration. Each contractile unit is separated by a dense body, see Fig. 1. The statistical dispersion of the orientation of the filament series in the micro-sphere in Fig. 3 is described by a density function $\rho = \rho(\mathbf{M})$, where $\rho(\mathbf{M})$ fulfils a normalisation criterion, say

$$\int_S \rho(\mathbf{M}) \mathrm{d}S = 1. \tag{5}$$

The density function is defined over some surface domain S, for example a half unit sphere.

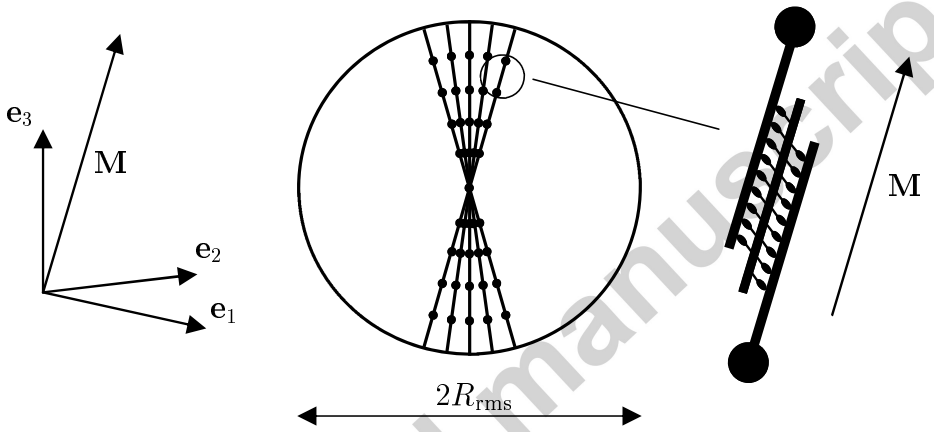

Figure 3: Representative micro-sphere with radius R_{rms}.

The mechanical behaviour of the myosin/actin units is modelled by use of an "active" dashpot in series with an elastic spring. The dashpot accounts for the relative sliding between myosin and actin filaments, and the spring accounts for the elasticity of the cross-bridges (the myosin and actin filaments themselves are considered rigid). A contractile filament is oriented in a direction defined by the vector $\mathbf{M}$. The stretching of the tissue in the direction of a contractile filament is denoted λ_{f} and is defined as $\lambda_{\mathrm{f}}^2 = \mathbf{MCM}$. Fig. 4 shows

a principle sketch of a contractile unit. In the undeformed configuration, the length of the unit is L_{cu}. In the deformed state, the length of the contractile unit has changed to $\lambda_{\mathrm{f}} \cdot L_{\mathrm{cu}}$. The myosin and actin filaments are treated as rigid bars, and the myosin filament has a length of L_{mf}. The stretch λ_{f} is decomposed according to $\lambda_{\mathrm{f}} = \lambda_{\mathrm{e}}\lambda_{\mathrm{fc}}$. The relative sliding between myosin and actin filaments is accounted for by λ_{fc}, and λ_{e} accounts for the elastic stretching of the cross-bridges. (Index "fc" stands for filament contraction.) The strain energy for the contractile apparatus is computed as the strain energy per unit reference volume of the representative micro-sphere, according to:

$$\begin{aligned} \Psi_{\mathrm{a}} &= \frac{1}{V_{\mathrm{rms}}} \int_S \rho(\mathbf{M}) N_{\mathrm{cu}} V_{\mathrm{rms}} \frac{\mu_{\mathrm{cu}}(n_3+n_4)}{4} \left(\lambda_{\mathrm{e}}^2(\mathbf{M}) - 1\right)^2 \mathrm{d}S = \\ &= \frac{\mu_{\mathrm{a}}}{4}(n_3+n_4) \int_S \rho(\mathbf{M}) \left(\frac{\mathbf{MCM}}{\lambda_{\mathrm{fc}}^2(\mathbf{M})} - 1 \right)^2 \mathrm{d}S, \end{aligned} \tag{6}$$

where $V_{\mathrm{rms}} = 4\pi R_{\mathrm{rms}}^3/3$ is the volume of the micro-sphere, μ_{cu} is the stiffness that an actin/myosin unit will exhibit if all cross-bridges are attached, N_{cu} is the number of contractile (myosin/actin) units per unit reference volume, and $\mu_{\mathrm{a}} = \mu_{\mathrm{cu}} N_{\mathrm{cu}}$. The factor $(\lambda_{\mathrm{e}}^2(\mathbf{M}) - 1)^2$ accounts for the strain energy stored in the cross-bridges. The exponent 2 outside the brackets is necessary because stresses, which are obtained by differentiation of Eq. (6), should also be zero for $\lambda_{\mathrm{e}} = 1$. The factor $(n_3 + n_4)$ accounts for the fraction of cross-bridges that are attached and thus contribute to the stiffness of the filaments. Only cross-bridges in states s_3 and s_4 are attached, and these two types of cross-bridges are assumed to have the same elastic stiffness. Note that, since the overlap between actin and myosin filaments is constant (L_{mf})

for moderate contractions, the number of cross-bridges that may contribute to force generation depends only on the activation level $(n_3 + n_4)$.

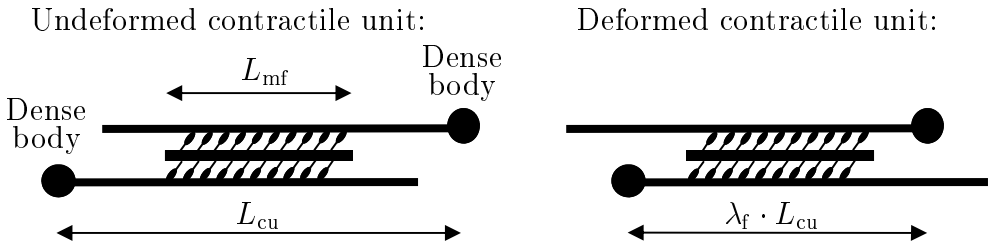

Figure 4: Undeformed and deformed contractile unit.

The thermomechanical state of the contractile apparatus is thus determined by the state variables n_3, n_4, $\mathbf{C}$, and $\lambda_{\mathrm{fc}}(\mathbf{M})$. Note that $\lambda_{\mathrm{fc}}(\mathbf{M})$ is a function of the orientation vector $\mathbf{M}$, and that anisotropic muscle contraction therefore is possible.

The resulting second Piola-Kirchhoff stress for the active part is

$$\mathbf{S}_{\mathrm{a}} = \mu_{\mathrm{a}}(n_3 + n_4) \int_S \rho(\mathbf{M}) \left(\frac{\mathbf{M}\mathbf{C}\mathbf{M}}{\lambda_{\mathrm{fc}}^2(\mathbf{M})} - 1 \right) \frac{\mathbf{M} \otimes \mathbf{M}}{\lambda_{\mathrm{fc}}^2(\mathbf{M})} \mathrm{d}S - p_{\mathrm{a}} \mathbf{C}^{-1}. \qquad (7)$$

An evolution equation for $\lambda_{\mathrm{fc}}(\mathbf{M})$ is required. The internal mechanical dissipation per unit reference volume is defined as $D_{\mathrm{int}} = P_{\mathrm{ext}} - \dot{\Psi}|_{\mathbf{n}}$, where P_{ext} is the external mechanical power imposed on the volume and $\dot{\Psi}|_{\mathbf{n}}$ is the associated increase in free energy for a given (constant) chemical state. External work is imposed in terms of the external stress $\mathbf{P}$ and in terms of the work performed by the cross-bridges in the smooth muscle. It is assumed that the active contracting force from the cross-bridges in a myosin/actin unit is $T = T(n_3, n_4)$. The external power input can then be expressed as

$$P_{\mathrm{ext}} = \mathbf{P} : \dot{\mathbf{F}} + \frac{1}{V_{\mathrm{rms}}} \int_S \rho(\mathbf{M}) N_{\mathrm{cu}} V_{\mathrm{rms}} T L_{\mathrm{cu}} \dot{\lambda}_{\mathrm{fc}}(\mathbf{M}) \mathrm{d}S. \qquad (8)$$

The increase in free energy can be expressed as

$$\dot{\Psi}|_{\mathbf{n}} = \frac{\partial \Psi}{\partial \mathbf{F}} : \dot{\mathbf{F}} - \mu_{\mathrm{a}}(n_3 + n_4) \int_S \rho(\mathbf{M}) \left(\frac{\mathbf{MCM}}{\lambda_{\mathrm{fc}}^2(\mathbf{M})} - 1 \right) \frac{\mathbf{MCM}}{\lambda_{\mathrm{fc}}^3(\mathbf{M})} \dot{\lambda}_{\mathrm{fc}}(\mathbf{M}) \mathrm{d}S. \quad (9)$$

Making use of the definition $\mathbf{P} = \partial \Psi / \partial \mathbf{F}$, D_{int} may be expressed as

$$D_{\mathrm{int}} = \int_S \rho(\mathbf{M}) \left\{ \bar{P}_{\mathrm{cr}} + \mu_{\mathrm{a}}(n_3 + n_4) \left(\frac{\mathbf{MCM}}{\lambda_{\mathrm{fc}}^2(\mathbf{M})} - 1 \right) \frac{\mathbf{MCM}}{\lambda_{\mathrm{fc}}^3(\mathbf{M})} \right\} \dot{\lambda}_{\mathrm{fc}}(\mathbf{M}) \mathrm{d}S \geq 0, \quad (10)$$

where the definition $\bar{P}_{\mathrm{cr}} = N_{\mathrm{cu}} T L_{\mathrm{cu}}$ has been introduced. An evolution equation for $\lambda_{\mathrm{fc}}(\mathbf{M})$ is now adopted according to

$$\eta \dot{\lambda}_{\mathrm{fc}}(\mathbf{M}) = \bar{P}_{\mathrm{cr}} + R(\mathbf{M}), \quad (11)$$

where η is a positive material parameter, and the reaction stress R is

$$R(\mathbf{M}) = \mu_{\mathrm{a}}(n_3 + n_4) \left(\frac{\mathbf{MCM}}{\lambda_{\mathrm{fc}}^2(\mathbf{M})} - 1 \right) \frac{\mathbf{MCM}}{\lambda_{\mathrm{fc}}^3(\mathbf{M})}. \quad (12)$$

(For an introduction to thermodynamics, see for example Holzapfel (2000).) For this choice of evolution equation, the integrand in Eq. (10) always becomes non-negative, and thermodynamic consistency is ensured. We emphasise that Eq. (11) is the evolution law not just for a single-valued variable but for the *function* $\lambda_{\mathrm{fc}}(\mathbf{M})$.

It is the stress $\bar{P}_{\mathrm{cr}}$ that causes muscle contraction, and $\bar{P}_{\mathrm{cr}}$ should be interpreted as an average contractile stress caused by the cross-bridges in the myosin/actin units. It is assumed that only cross-bridges in state s_3 contribute to filament contraction, i.e. actual contractile sliding between the myosin and actin filaments. However, when the cycling cross-bridges are too weak to contract the filaments further, attached (but non-cycling) cross-bridges in state s_4 will assist the cycling cross-bridges in state s_3 in preventing backsliding in the contractile filaments.

When the total resistance from cycling and non-cycling cross-bridges is weaker than R in Eq. (11), the non-cycling cross-bridges in state s_4 break and no longer contribute to the strength of the filament. Cross-bridges in state s_3 may also break, but since they cycle relatively fast, they will continuously reattach to the actin filaments, and thereby continue to resist (i.e. slow down) the extension of the contractile filament. The processes outlined above are accounted for by using an active stress $\bar{P}_{\rm cr}$ on the following form:

$$\begin{aligned} \bar{P}_{\rm cr} &= -\kappa_3 n_3, \quad \text{for} \quad \kappa_3 n_3 \geq R(\mathbf{M}), \\ \bar{P}_{\rm cr} &= -R(\mathbf{M}), \quad \text{for} \quad \kappa_3 n_3 < R(\mathbf{M}) \leq \kappa_3 n_3 + \kappa_4 n_4, \\ \bar{P}_{\rm cr} &= -\kappa_3 n_3, \quad \text{for} \quad \kappa_3 n_3 + \kappa_4 n_4 < R(\mathbf{M}). \end{aligned} \tag{13}$$

Above κ_3 and κ_4 are material parameters related to the driving force of cycling cross-bridges in state s_3 and the passive strength of cross-bridges in state s_4, respectively. Thus, in the intermediate range $\kappa_3 n_3 < R(\mathbf{M}) \leq \kappa_3 n_3 + \kappa_4 n_4$, no sliding occurs in filaments oriented along $\mathbf{M}$, implying $\dot{\lambda}_{\rm fc}(\mathbf{M}) = 0$ (but sliding may well occur in filaments oriented in other directions).

We may then summarise the parameters in the active part of the mechanical model: four material constants $\mu_{\rm a}$, κ_3, κ_4, and η, one statistical distribution for the contractile apparatus $\rho(\mathbf{M})$, and one internal variable function $\lambda_{\rm fc}(\mathbf{M})$.

3.3. Passive mechanical response

The passive term $\Psi_{\rm p}$ in Eq. (2) pertains to the passive response of the muscle cells and their physiological surrounding, such as extracellular proteins. In general, soft biological tissues appear to have a viscous component

in their constitutive response. However, in the present study the main focus is on the relatively slow activation of the contractile apparatus in smooth muscle, and the passive behaviour is therefore considered to be purely elastic. Thus, a neoHookean model is adopted for Ψ_{p} according to

$$\Psi_{\mathrm{p}} = \frac{\mu_{\mathrm{p}}}{2}(\mathbf{C} : \mathbf{I} - 3), \tag{14}$$

where $\mathbf{I}$ is the identity tensor and μ_{p} is the stiffness of the passive components in the tissue.

The contribution to the second Piola-Kirchhoff stress from the passive part becomes

$$\mathbf{S}_{\mathrm{p}} = \mu_{\mathrm{p}}\mathbf{I} - p_{\mathrm{p}}\mathbf{C}^{-1}. \tag{15}$$

4. Model formulation for uniaxial tension and axisymmetric myosin filament distribution

4.1. Deformation state in uniaxial tension

The proposed constitutive model for smooth muscle tissue is compared to experimental results for smooth muscle from swine carotid media. In these experimental investigations, uniaxial tensile tests of tissue specimens are performed. A uniaxial formulation of the proposed model is therefore derived in this section.

It is assumed that the material behaviour is transversely isotropic with $\mathbf{e}_3$ defining the axis of symmetry. The tissue is exposed to uniaxial tension, where the force is applied in the $\mathbf{e}_3$-direction. The resulting deformation state can then be expressed as

$$\mathbf{F} = \lambda_1\mathbf{e}_1 \otimes \mathbf{e}_1 + \lambda_2\mathbf{e}_2 \otimes \mathbf{e}_2 + \lambda_3\mathbf{e}_3 \otimes \mathbf{e}_3. \tag{16}$$

Due to symmetry and incompressibility, $\lambda_1 = \lambda_2 = 1/\sqrt{\lambda_3}$. The homogeneous mechanical state is then fully characterised by the stretch λ_3 together with a single function $\lambda_{\rm fc}(\mathbf{M})$.

4.2. Axisymmetric distribution of contractile filaments

The unit vector $\mathbf{M}$ is defined by use of spherical coordinates θ and ϕ, i.e. $\mathbf{M} = \sin\theta\cos\phi\mathbf{e}_1 + \sin\theta\sin\phi\mathbf{e}_2 + \cos\theta\mathbf{e}_3$, see Fig. 5(a). We assume that the density function $\rho(\mathbf{M})$ is axisymmetric with respect to the $\mathbf{e}_3$-direction, i.e. $\rho = \rho(\theta)$. The following density function is used:

$$\begin{aligned} \rho(\theta) &= c(a^2 - \theta^2) \quad \text{for} \quad 0 \leq \theta \leq a, \\ \rho(\theta) &= 0 \quad \text{otherwise.} \end{aligned} \tag{17}$$

The density function is defined over the upper half of a unit sphere, i.e. for $\theta \in [0, \pi/2]$, $\phi \in [0, 2\pi]$, and it is subject to the normalisation

$$\int_{\theta=0}^{\pi/2} \int_{\phi=0}^{2\pi} \rho(\theta)\sin\theta \mathrm{d}\phi\mathrm{d}\theta = 2\pi \int_{\theta=0}^{\pi/2} \rho(\theta)\sin\theta\mathrm{d}\theta = 1. \tag{18}$$

Thus, the variance of the filament dispersion is set by a, and c is adjusted so that the normalisation condition in Eq. (18) is fulfilled.

4.3. Stress components

For the transversely isotropic material exposed to uniaxial tension considered here, the first Piola-Kirchhoff stresses P_{11} and P_{22} may be expressed as

$$\begin{aligned} P_{11} &= P_{22} = \frac{\mu_{\rm p}}{\sqrt{\lambda_3}} + \\ &+ \frac{\pi\mu_{\rm a}(n_3 + n_4)}{\sqrt{\lambda_3}} \int_{\theta=0}^{\pi/2} \rho(\theta) \left(\frac{\mathbf{MCM}}{\lambda_{\rm fc}^4(\theta)} - \frac{1}{\lambda_{\rm fc}^2(\theta)} \right) \sin^3\theta \mathrm{d}\theta - \\ &- (p_{\rm p} + p_{\rm a})\sqrt{\lambda_3}. \end{aligned} \tag{19}$$

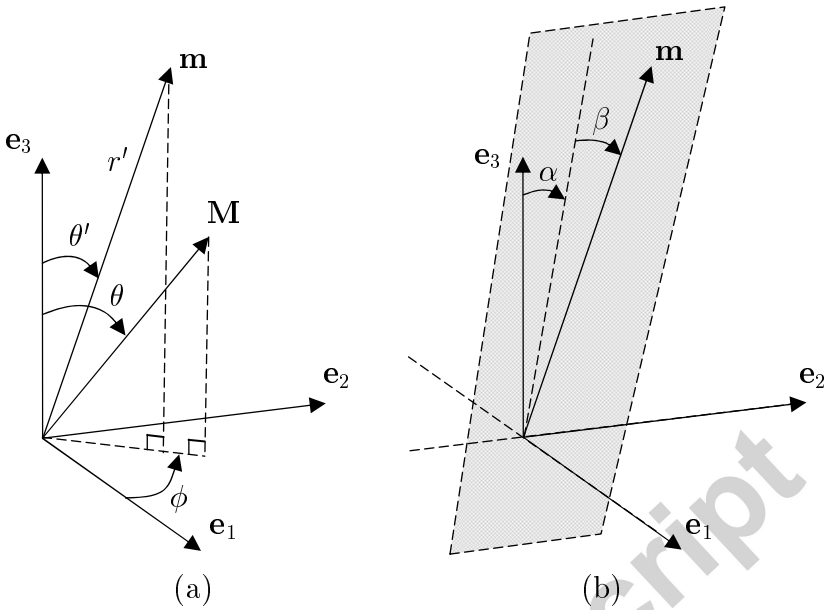

Figure 5: (a) Spherical coordinates used to describe vectors $\mathbf{M}$ and $\mathbf{m}$. (b) Alternative angular coordinates α and β used to describe the conditional density function for contractile filaments in the deformed configuration. The indicated plane is defined by the basis vector $\mathbf{e}_2$ and $\mathbf{m}$, and α is the angle between basis vector $\mathbf{e}_3$ and this plane. The angle β is the angle between $\mathbf{m}$ and the $\mathbf{e}_1 - \mathbf{e}_3$-plane.

The boundary conditions $P_{11} = P_{22} = 0$ enable the determination of the Lagrange multipliers:

$$p_{\mathrm{a}} = \frac{\pi \mu_{\mathrm{a}} (n_3 + n_4)}{\lambda_3} \int_{\theta=0}^{\pi/2} \rho(\theta) \left(\frac{\mathbf{MCM}}{\lambda_{\mathrm{fc}}^4(\theta)} - \frac{1}{\lambda_{\mathrm{fc}}^2(\theta)} \right) \sin^3\theta \mathrm{d}\theta, \tag{20}$$

$$p_{\mathrm{p}} = \frac{\mu_{\mathrm{p}}}{\lambda_3}. \tag{21}$$

The first Piola-Kirchhoff stress in the $\mathbf{e}_3$-direction, P_{33}, then takes on the form

$$P_{33} = (\mathbf{P}_{\mathrm{p}})_{33} + (\mathbf{P}_{\mathrm{a}})_{33} = \mu_{\mathrm{p}} \left(\lambda_3 - \frac{1}{\lambda_3^2} \right) +$$

$$+ \quad \pi\mu_{\mathrm{a}}(n_3+n_4)\int_{\theta=0}^{\pi/2}\rho(\theta)\left(\frac{\mathbf{MCM}}{\lambda_{\mathrm{fc}}^4(\theta)}-\frac{1}{\lambda_{\mathrm{fc}}^2(\theta)}\right)\cdot \tag{22}$$

$$\cdot \quad \left(2\lambda_3\cos^2\theta\sin\theta-\frac{1}{\lambda_3^2}\sin^3\theta\right)\mathrm{d}\theta.$$

4.4. Conditional density function for filaments in deformed state

There are experimental results for the statistical distribution of myosin filaments in smooth muscle. In this histological examination, the distribution of myosin filaments in a single plane in the tissue is given. In order to facilitate a comparison between these experimental histological results and the proposed model, a conditional density function for the contractile filament distribution in a deformed state is now derived.

The density function ρ is a function of the unit vector $\mathbf{M}$. When loading the material uniaxially in the $\mathbf{e}_3$-direction, a unit vector $\mathbf{M}$ maps to the deformed vector $\mathbf{m}$ according to $\mathbf{m}=\mathbf{FM}$, see Fig. 5(a). The deformed vector may be expressed as $\mathbf{m}=r'\sin\theta'\cos\phi\mathbf{e}_1+r'\sin\theta'\sin\phi\mathbf{e}_2+r'\cos\theta'\mathbf{e}_3$, where $r'=|\mathbf{m}|$ and θ' are two new spherical coordinates. Note that the angle ϕ remains the same during the deformation. By use of the relations $\mathbf{m}=\mathbf{FM}$, $|\mathbf{m}\times\mathbf{e}_3|=|\mathbf{m}||\mathbf{e}_3|\sin\theta'$ and $\mathbf{m}\cdot\mathbf{e}_3=|\mathbf{m}||\mathbf{e}_3|\cos\theta'$, the angles θ and θ' may be related to each other as $\tan\theta=\lambda_3^{3/2}\tan\theta'$. Thus,

$$\theta=g(\theta')=\arctan(\lambda_3^{3/2}\tan\theta'). \tag{23}$$

Two stochastic variables, Θ and Θ', are now introduced, where Θ has the distribution function $F_\Theta(\theta)$ defined as

$$F_\Theta(\theta)=\int_{\bar\theta=0}^{\theta}\int_{\phi=0}^{2\pi}\rho(\bar\theta)\sin\bar\theta\,\mathrm{d}\phi\mathrm{d}\bar\theta=2\pi\int_{\bar\theta=0}^{\theta}\rho(\bar\theta)\sin\bar\theta\mathrm{d}\bar\theta, \tag{24}$$

where $\bar\theta$ is an integration variable. Thus, $F_\Theta(\theta)$ gives the probability of finding the stochastic variable Θ in the angular range $[0,\theta]$. The associated

density function $f_\Theta(\theta)$ is obtained by differentiation according to

$$f_\Theta(\theta) = \frac{\mathrm{d}F_\Theta}{\mathrm{d}\theta} = 2\pi\rho(\theta)\sin\theta. \tag{25}$$

The distribution function $F_{\Theta'}(\theta')$ for the stochastic variable Θ' gives the probability of finding a contractile filament in the deformed state in the angular range $[0, \theta']$. By use of Eqs. (23) and (24), $F_{\Theta'}(\theta')$ may be expressed as

$$F_{\Theta'}(\theta') = 2\pi \int_{\bar{\theta}=0}^{g(\theta')} \rho(\bar{\theta})\sin\bar{\theta}\mathrm{d}\bar{\theta}. \tag{26}$$

The density function is obtained by differentiation:

$$f_{\Theta'}(\theta') = \frac{\mathrm{d}F_{\Theta'}}{\mathrm{d}g(\theta')}\frac{\mathrm{d}g(\theta')}{\mathrm{d}\theta'} = 2\pi\rho(g(\theta'))\sin(g(\theta'))\frac{\mathrm{d}g(\theta')}{\mathrm{d}\theta'}. \tag{27}$$

The axisymmetric filament distribution in the deformed state may be characterised by a density function $\rho'(\theta')$. Using the same procedure as in Eq's. (24) and (25), $f_{\Theta'}(\theta')$ may also be expressed as

$$f_{\Theta'}(\theta') = 2\pi\rho'(\theta')\sin\theta'. \tag{28}$$

By use of Eq's. (27) and (28), $\rho'(\theta')$ may be identified as

$$\rho'(\theta') = \rho(g(\theta'))\frac{\sin(g(\theta'))}{\sin\theta'}\frac{\mathrm{d}g(\theta')}{\mathrm{d}\theta'}. \tag{29}$$

Two new angular coordinates, $\alpha \in [-\pi/2, \pi/2]$ and $\beta \in [-\pi/2, \pi/2]$, are now introduced, and in these coordinates the vector $\mathbf{m}$ is written $\mathbf{m} = r'\sin\alpha\cos\beta\mathbf{e}_1 + r'\sin\beta\mathbf{e}_2 + r'\cos\alpha\cos\beta\mathbf{e}_3$, see Fig. 5(b). Two associated stochastic variables, A and B, are introduced, and the distribution function for these variables is

$$F_{A,B}(\alpha, \beta) = \int_{\bar{\alpha}=-\pi/2}^{\alpha}\int_{\bar{\beta}=-\pi/2}^{\beta} \rho'(\theta'(\bar{\alpha}, \bar{\beta}))\cos\bar{\beta}\mathrm{d}\bar{\beta}\mathrm{d}\bar{\alpha}, \tag{30}$$

where $\theta'(\alpha,\beta) = \arccos(\cos\alpha\cos\beta)$, and $\bar{\alpha}$ and $\bar{\beta}$ are integration variables. The associated density function is

$$f_{A,B}(\alpha,\beta) = \frac{\partial^2 F_{A,B}(\alpha,\beta)}{\partial\alpha\partial\beta} = \rho'(\theta'(\alpha,\beta))\cos\beta. \tag{31}$$

The conditional density function $f_{A|B=0}(\alpha)$ is then computed as

$$f_{A|B=0}(\alpha) = \frac{f_{A,B}(\alpha,\beta=0)}{f_B(\beta=0)} = \frac{\rho'(|\alpha|)}{\int_{\bar{\alpha}=-\pi/2}^{\pi/2}\rho'(|\bar{\alpha}|)\mathrm{d}\bar{\alpha}}, \tag{32}$$

where $f_B(\beta)$ is the marginal density function of B. Note that for $\beta = 0$, the expression for θ' simplifies to $\theta' = |\alpha|$. The value of $\rho'(|\alpha|)$ is obtained by evaluating Eq. (29) for $\theta' = |\alpha|$. The conditional density function Eq. (32) will be used for comparison with experimental results.

4.5. Discretisation

Time was discretised using a constant time increment Δt. For a computed state i, the chemical state is defined by the variables $n_{1,i}$, $n_{2,i}$, $n_{3,i}$, and $n_{4,i}$. The evolution equation for the chemical state (1) is independent of the mechanical state, and an Euler forward algorithm according to

$$\mathbf{n}_{i+1} = \mathbf{n}_i + \Delta t\mathbf{K}\mathbf{n}_i \tag{33}$$

is adopted, where the vector $\mathbf{n}_{i+1}$ holds the updated chemical state variables for state $i+1$.

The deformation at the computational state i is defined by $\lambda_{3,i}$ together with discrete values of the function $\lambda_{\mathrm{fc}}(\mathbf{M})$. In general, the function $\lambda_{\mathrm{fc}}(\mathbf{M})$ needs to be discretised and integrated over the (half) unit sphere (cf. Alastrue et al., 2009; Bazant and Oh, 1986; Miehe et al., 2004), but due to the axisymmetry in the present problem formulation, a discretisation in θ is enough.

Thus, the function $\lambda_{\mathrm{fc}}(\theta)$ is represented by the discrete values $\lambda_{\mathrm{fc}}^1 \ldots \lambda_{\mathrm{fc}}^{n_{\mathrm{int}}}$, where n_{int} is the number of integration points used. The associated angles $\theta^1 \ldots \theta^{n_{\mathrm{int}}}$ were distributed according to

$$\theta^k = (k - 1/2)\Delta\theta, \tag{34}$$

where $\Delta\theta = \pi/(2n_{\mathrm{int}})$. The evolution equation (11) was discretised and evaluated for each λ_{fc}^k according to

$$\lambda_{\mathrm{fc},i+1}^k = \lambda_{\mathrm{fc},i}^k + \frac{\Delta t}{\eta}(\bar{P}_{\mathrm{cr},i} + R_i(\theta^k)), \tag{35}$$

where the reaction force R is evaluated for the angle θ^k. When evaluating P_{33}, Eq. (22) was discretised using the integration points defined by Eq. (34).

5. Comparison with experiments on smooth muscle from media of swine carotid artery

The model is now compared to experimental data from smooth muscle tissue from the media of swine carotid arteries. Histological data for myosin filament dispersion was obtained from Walmsley and Murphy (1987) and tensile test data from Rembold and Murphy (1990b).

5.1. Histological data

Walmsley and Murphy (1987) perform histological examinations of the structural organisation of myosin filaments and dense bodies of smooth muscle from the media of swine carotid arteries. They study cross-sections of media rings as illustrated in Fig. 6, and determine the distribution of the angle α, defined as the angle between the circumferential direction and the myosin

filament. Assuming that the distribution of myosin filaments is axisymmetric with respect to the circumferential direction, the model distribution $\rho(\theta)$ may be compared to the experimental distribution of myosin filaments. Since Walmsley and Murphy (1987) investigate the distribution of myosin filaments within a cross-sectional plane, the conditional density function $f_{A|B=0}(\alpha)$ in Eq. (32) is the appropriate means of comparison.

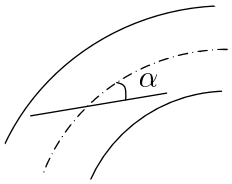

Figure 6: Principle sketch of cross-section of media ring from carotid artery. The angle α is defined as the angle between a myosin filament and the circumferential direction in the cross-sectional plane.

The circumferential direction in Walmsley and Murphy (1987) corresponds to the $\mathbf{e}_3$-direction in the present study. Walmsley et al. investigate the filament dispersion for two different (circumferential) stretches, corresponding to $\lambda_3 = 1.17$ and $\lambda_3 = 1.67$. (The specimens were fixed chemically to enable mechanical dissection and microstructural investigation.) In Fig. 7, histological data for the two different stretches considered by Walmsley et al. is compared with model predictions in terms of the conditional density function $f_{A|B=0}(\alpha)$. Model predictions are shown for $a \to 0$, $a = 0.44$ rad, $a = 1.66$ rad, and $a \to \infty$. The dispersion parameter $a = 0.44$ rad provides the best agreement with histological data. For this case, the dispersion of myosin filaments is accurately predicted for both $\lambda_3 = 1.17$ and $\lambda_3 = 1.67$.

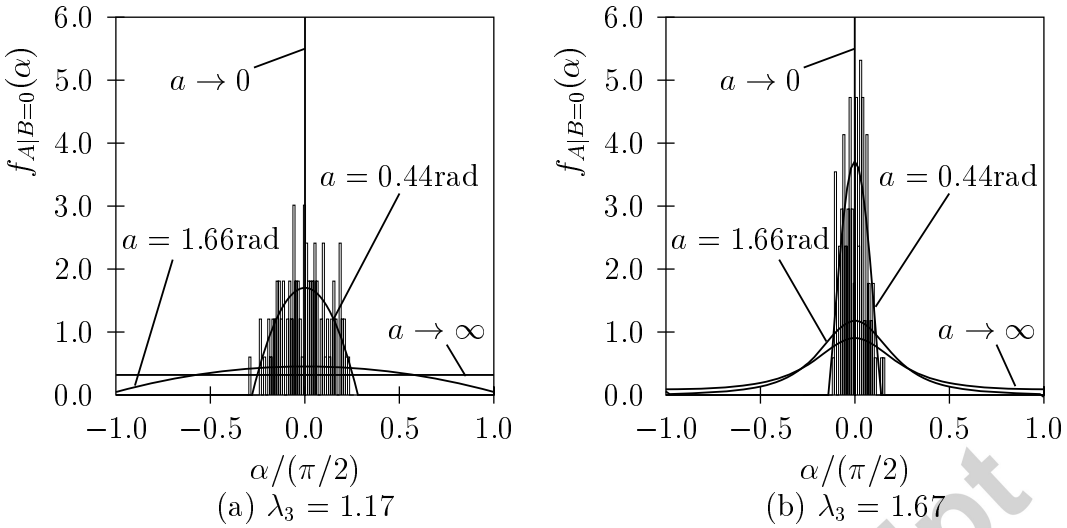

Figure 7: Conditional density function $f_{A|B=0}(\alpha)$ for stretches (a) $\lambda_3 = 1.17$ and (b) $\lambda_3 = 1.67$. Histological data from Walmsley and Murphy (1987) (bars) are shown together with model predictions (solid lines) for four values of the dispersion parameter a.

The distributions for $a \to 0$ (perfectly aligned myosin filaments) and $a \to \infty$ (isotropic distribution) are included as references.

5.2. Isometric tensile test results

In the tensile tests on smooth muscle from swine carotid media performed by Rembold and Murphy (1990b), the test specimens were about 1cm long and the long axis of the test specimens coincided with the circumferential direction of the original artery. The muscle tissue was activated by histamine, and specimens were exposed to isometric (constant length) tensile testing. Tests were performed at a temperature of 37°C.

When simulating the isometric tensile tests, a constant time increment of $\Delta t = 0.1$s was used. For the function λ_{fc}, a total number of $n_{\text{int}} = 20$ integration points were used. Further refinement of the spatial and time discretisa-

tions did not change the outcome significantly, and this level of discretisation was therefore considered adequate to give discretisation-independent results.

For the chemical model, described in Eq. (1), rate constants for swine carotid media smooth muscle were obtained from Hai and Murphy (1988), yielding $k_2 = k_5 = 0.5$, $k_3 = 4k_4$, $k_4 = 0.11$, and $k_7 = 0.01$. The two remaining rate constants k_1 and k_6 depend on the intracellular calcium ion concentration in the smooth muscle cells. For a specific value of $[Ca^{2+}]$, k_1 and k_6 may be determined by use of the steady-state stress in an isometric test, since k_1 and k_6 govern the steady-state fraction of force-generating cross-bridges in states s_3 and s_4. By use of results for the steady-state isometric stress in Rembold and Murphy (1990b), the estimates $k_1 = k_6 = 0.045$ were obtained.

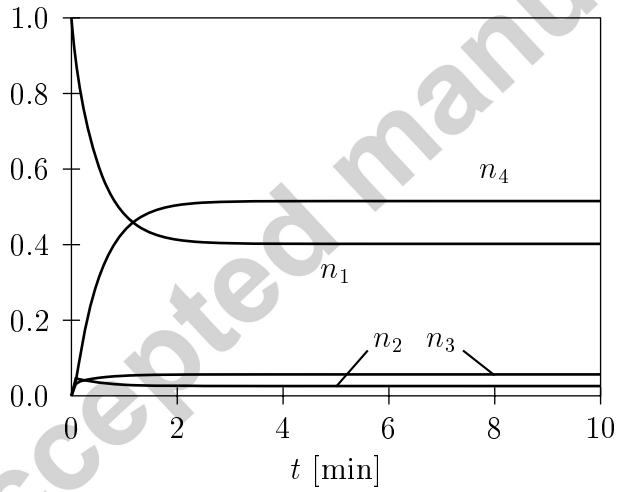

Figure 8: Predicted evolution of the state variables n_1, n_2, n_3, and n_4 in an isometric test in Rembold and Murphy (1990b).

In the isometric tensile test, the total first Piola-Kirchhoff stress (P_{33})

is registered as a function of time. The increase in stress depends both on the evolution of the chemical state variables n_1, n_2, n_3, n_4 and on the mechanical state function $\lambda_{\mathrm{fc}}(\mathbf{M})$. It is assumed, that at time $t = 0$, the contractile apparatus of the muscle tissue is completely inactivated (relaxed), corresponding to the states $n_1 = 1$, $n_2 = n_3 = n_4 = 0$, $\lambda_{\mathrm{fc}}(\mathbf{M}) = \sqrt{\mathbf{MCM}}$, where $\mathbf{C} = 1/\lambda_3(\mathbf{e}_1 \otimes \mathbf{e}_1 + \mathbf{e}_2 \otimes \mathbf{e}_2) + \lambda_3^2 \mathbf{e}_3 \otimes \mathbf{e}_3$. At time $t = 0$, the muscle is activated by histamine, which causes an increase in intracellular calcium ion concentration. The predicted evolution of the chemical state variables in the isometric tests is illustrated in Fig. 8. The chemical state variables stabilise at their equilibrium levels roughly after 2 min. At steady-state, most of the cross-bridges are predicted to be in state s_4, where they contribute to force generation in the latch-state. The fraction of cross-bridges in state s_3 that actively contributes to muscle contraction is estimated to be relatively small, about 5%.

Rembold and Murphy (1990b) perform isometric tests for the two different stretches $\lambda_3 = 1.17$ and 1.67. Based on the information on the passive behaviour of the tissue provided by Rembold and Murphy (1990b), the passive stiffness was estimated to $\mu_{\mathrm{p}} = 14.1\mathrm{kPa}$. In Fig. 9, the resulting evolution of stress is shown together with model predictions. Since both of the stretches considered deviate from the load-free configuration of Ψ_{p}, there will be a contribution from the passive stiffness in P_{33}. Experimental results are indicated by symbols and model predictions by lines. Different values of the dispersion parameter a are investigated. For each value of a, the model parameters μ_{a}, κ_3 and η were chosen to give the best fit to the stress data for $\lambda_3 = 1.17$, and the curve for $\lambda_3 = 1.67$ was thereafter predicted. Thus,

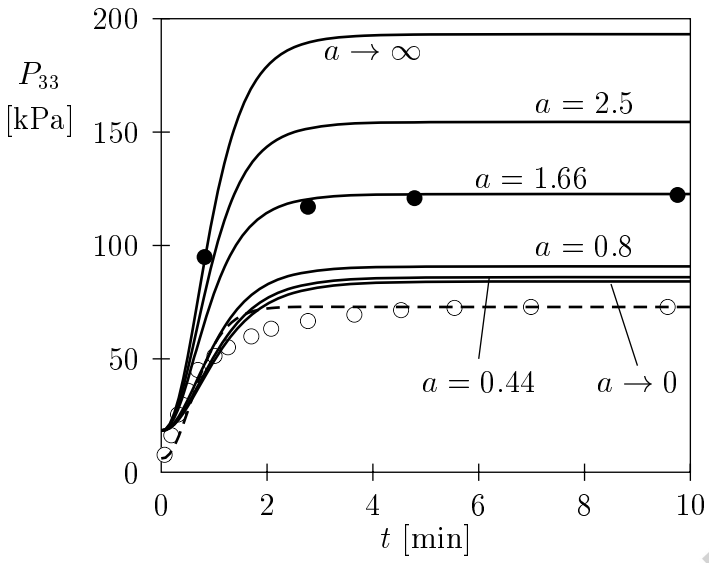

Figure 9: Evolution of stress P_{33} in isometric tests. Experimental isometric test results are shown for $\lambda_3 = 1.17$ (open symbols) and $\lambda_3 = 1.67$ (filled symbols). Model predictions are shown for $\lambda_3 = 1.17$ (dashed line) using $a = 1.66$ rad, and for $\lambda_3 = 1.67$ (solid lines) using $a \to 0$, $a = 0.44$ rad, $a = 0.8$ rad, $a = 1.66$ rad, $a = 2.5$ rad, and $a \to \infty$.

each value of a has its own set of μ_{a}, κ_3, η associated with it, and these sets are summarised in Table 1. The information from a single isometric test is not enough to uniquely determine all three of these model parameters, and a fixed ratio $\mu_{\mathrm{a}}/\kappa_3 = 1$ was therefore assumed. This ratio governs the magnitude of change in λ_{fc} during muscle contraction, where an increasing ratio tends to decrease the change in λ_{fc}. (If κ_3 becomes too large compared to μ_{a}, it will result in values of λ_{fc} that correspond to cross-bridge deformations that are too large to be physically plausible.) Since only isometric tests are performed, the fourth model parameter κ_4 never comes into play and can therefore not be determined.

The fittings to the stress data for $\lambda_3 = 1.17$ were virtually identical for the

different values of a, and the dashed line in Fig. 9 pertains to $a = 1.66$. This value of a proved to give the best prediction of the stress data for $\lambda_3 = 1.67$.

Fig. 9 shows that the steady-state stress increases with increasing filament dispersion. The reason is that as the tissue deforms from $\lambda_3 = 1.17$ to $\lambda_3 = 1.67$, the contractile apparatus becomes more aligned in the $\mathbf{e}_3$-direction, and the force-generating capacity in this direction therefore increases. Thus, the increase in steady-state stress is a geometrical effect associated with large deformations. Interestingly, the curve for $a = 0.44$, which provided the best prediction for the histological data, severely underestimates the stress curve for $\lambda_3 = 1.67$. This will be further discussed subsequently.

Table 1: Model parameter sets for different levels of myosin filament dispersion.

a [rad]	μ_{a} [kPa]	κ_3 [kPa]	η [kPa·s]
0	1.23	1.23	41.1
0.44	1.33	1.33	44.3
0.8	1.59	1.59	53.0
1.66	4.21	4.21	140
2.5	7.31	7.31	244
∞	11.1	11.1	370

In Table 1, parameters μ_{a}, κ_3 and η increase with dispersion a. Thus, in order to be able to generate the same steady-state stress in uniaxial tension for increasing myosin filament dispersion, the stiffness and strength of the contractile filament fabric need to increase, which is reflected by the increase

in μ_a and κ_3. This may be thought of as either an increase in cross-bridge stiffness/strength or an increase in the number of contractile units per unit volume. At the same time, the initial rate of stress increase in the isometric test should be maintained, which requires that η increases with μ_a and κ_3.

The evolution of the function λ_{fc} is now considered in some more detail, and since $a = 1.66$rad provided the best fit to the isometric test data, this case is investigated further. A total number of $n_{int} = 20$ integration points were used, corresponding to the state variables $\lambda_{fc}^1 \ldots \lambda_{fc}^{20}$. Thus, the variable λ_{fc}^1 is associated with muscle contraction in the $\mathbf{e}_3$-direction, λ_{fc}^{20} with contraction in the $\mathbf{e}_1$-$\mathbf{e}_2$-plane, and λ_{fc}^{10} with the 45°-direction in-between. (To be more specific, these three state variables pertains to the directions $\theta^1 = 0.039$ rad, $\theta^{10} = 0.75$ rad, and $\theta^{20} = 1.53$ rad, respectively.) Fig. 10 shows the evolution of these state variables for the two isometric test cases. For both values of λ_3, λ_{fc}^1 and λ_{fc}^{10} start at values greater than 1, whereas λ_{fc}^{20} starts below 1. This is due to the fact that stretches $\lambda_3 > 1$ cause contraction in the transverse directions due to assumed incompressibility of the tissue. As the muscle is activated, all values of λ_{fc} decrease and stabilise after about 2 min. Thus, the mechanical part of the constitutive model stabilises at about the same time as the state variables n_1-n_4, see Fig. 8.

As the muscle is activated, the value of λ_{fc} decreases in all directions. This is further illustrated in Fig. 11, where initial and steady-state distributions of λ_{fc} are shown for the two stretch cases. The case for $\lambda_3 = 1.67$ shows a greater variation both in initial distribution and in steady-state distribution of λ_{fc}. This is due to the higher value of λ_3 and the associated higher degree of transverse contraction. For $\lambda_3 = 1.17$, the contraction is fairly uniformly

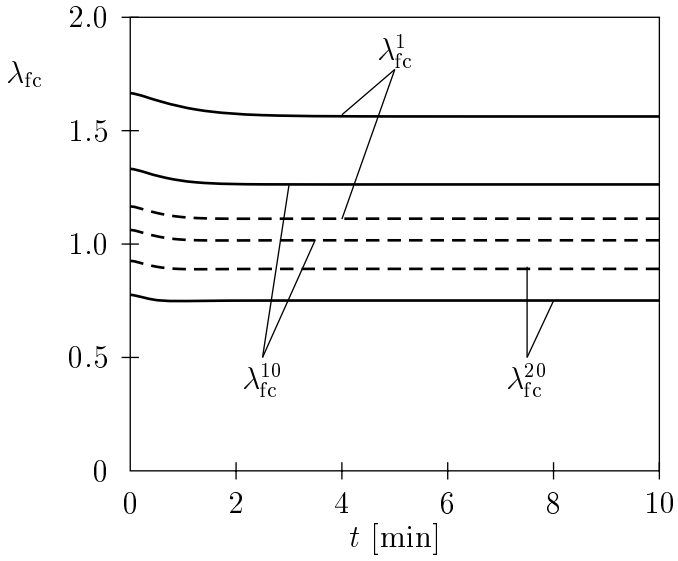

Figure 10: Predicted evolution of λ_{fc} in the isometric tests for $\lambda_3 = 1.17$ (dashed lines) and $\lambda_3 = 1.67$ (solid lines). Solutions are shown for λ_{fc} corresponding to directions $\theta^1 = 0.039$ rad (essentially the loading direction), $\theta^{10} = 0.75$ rad (45°-direction), and $\theta^{20} = 1.53$ rad (perpendicular to loading direction). Dispersion parameter: $a = 1.66$.

distributed over θ, whereas for $\lambda_3 = 1.67$, the contraction is clearly localised in the direction of loading ($\theta = 0$).

6. Discussion

A new constitutive model for the biomechanical behaviour of smooth muscle tissue is proposed. The model is based on a previously proposed approach by Kroon (2010a), which has now been expanded to include effects of myosin filament dispersion. The model includes the active as well as the passive components of smooth muscle response. The active part includes a chemical model (Hai and Murphy, 1988), accounting for the cross-bridge cycling that is the driving mechanism in smooth muscle contraction, and a

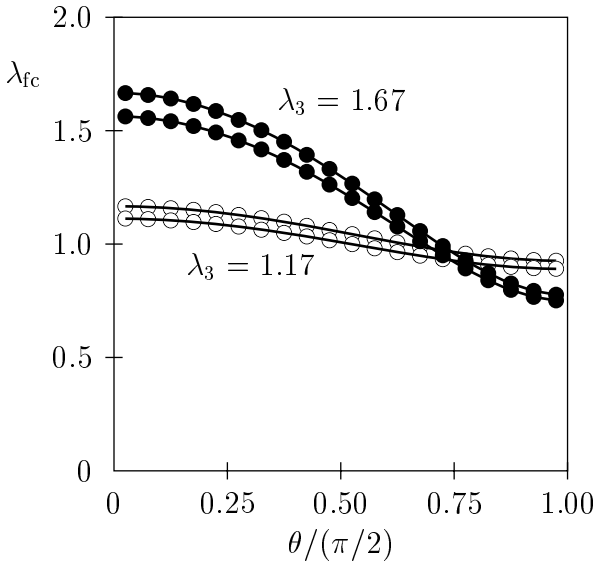

Figure 11: Predicted distribution of λ_{fc} in the isometric tests for $\lambda_3 = 1.17$ (open symbols) and $\lambda_3 = 1.67$ (filled symbols). Initial distributions ($t = 0^+$) are located above the steady-state distributions ($t \to \infty$) for the two stretch cases, respectively. Dispersion parameter: $a = 1.66$.

mechanical model based on Hill's three-component model (Hill, 1938). In the active part of the model, the cytosolic $[Ca^{2+}]$ is the in-signal that triggers cross-bridge cycling, which causes a contraction of the contractile apparatus in the cells and thereby contraction of the muscle tissue.

Contraction of smooth muscle tissue involves a chain of electrical, biochemical and mechanical events. Previous models have attempted to describe different parts of this chain. For example, Rosenbluth (1965), Fay and Delise (1973), and Herrera et al. (2005) mainly attempted to describe the structural organisation of the contractile apparatus in smooth muscle cells and how and where contractile filaments were attached to the cell membrane. A few studies (e.g. Miftakhov and Abdusheva (1996)) have focused on the elec-

trical/biochemical couplings associated with smooth muscle activation. Mechanical modelling of smooth muscle has been dominated by Hill's approach (Hill, 1938) and variants thereof (e.g. Gestrelius and Borgström (1986) and Yang et al. (2003a)). A few other approaches exist, though, for example Lee and Schmid-Schönbein (1996b), who assume that the effect of muscle activation can be modelled in a phenomenological sense by changing the reference configuration of the (passive) tissue. Rachev and Hayashi (1999) and Zulliger et al. (2004) use a slightly similar approach. They include the effects of the contractile apparatus explicitly, and muscle activation is taken to change the reference configuration of the contractile units. However, in these models, only mechanical aspects of smooth muscle contraction are modelled explicitly, and no biochemistry is included. The model proposed by Stålhand et al. (2008) includes both a biochemical component (i.e. Hai and Murphy's four-state model (Hai and Murphy, 1988)) and a mechanical part with the same basic components as Gestrelius and Borgström (1986). The model proposed by Yang et al. (2003a,b) appears to be the most ambitious so far, since it includes the whole chain from electrical activation, the biochemical processes thus triggered, and the eventual mechanical contraction of the contractile apparatus. In two studies, related to the present work, uniaxial (Murtada et al., 2010a) and multiaxial (Murtada et al., 2010b) contraction of smooth muscle were modelled. In the model allowing for multiaxial muscle contraction, a statistical distribution for the orientation of contractile units was introduced, but isotropic filament contraction was assumed, i.e. contractile units with different orientations contracted equally. In the present study, anisotropic muscle contractions are modelled. The outcome in terms of uniaxial iso-

metric stress behaviour does not differ much from the previous study with isotropic contractions (Murtada et al., 2010b).

The model proposed here is fairly simple, and the model parameters have quite clear physical interpretations. The stiffness μ_{a} is related to the elastic stiffness of the contractile apparatus. This includes first of all the elasticity of the cross-bridges and the density of contractile units per unit cross-sectional area. The assumption is made that cross-bridges in states s_3 and s_4 have the same stiffness. The parameters κ_3 and κ_4 are related to the driving force and strength of the cycling and non-cycling cross-bridges, respectively. Only cross-bridges in state s_3 actively contribute to sliding between myosin and actin filaments, but cross-bridges in state s_4 help cross-bridges in state s_3 to prevent back-sliding (reversed contraction). Finally, the dispersion parameter a describes the statistical scatter in the orientation of myosin filaments.

The model accounts for the fact that myosin filaments and the associated dense bodies exhibit a statistical dispersion in their orientation in space. This dispersion has been verified in at least one histological examination (Walmsley and Murphy, 1987). The influence of this dispersion on the mechanical behaviour of the tissue has been demonstrated in the present paper. An axisymmetric density function was adopted for the filament dispersion, and when compared to the experimental results for smooth muscle from arterial media (Walmsley and Murphy, 1987), the adopted density function was fully able to describe the dispersions of myosin filaments obtained from histological examinations at two different uniaxial stretches. The model was also able to predict the stress data in isometric tensile tests. However, the dispersion estimated from histological data ($a = 0.44$ rad) was not the dispersion that

gave the best prediction in the isometric tensile tests, but a higher degree of dispersion ($a = 1.66$ rad) was required to predict the steady-state stress level at the higher stretch. There are two probable explanations for this anomaly. One explanation could be that the filament dispersion in the longitudinal direction of the carotid artery is significantly larger than the dispersion in the thickness direction (which was quantified in the histological examination by Walmsley and Murphy (1987)), and that the assumption of an axisymmetric filament dispersion therefore is unrealistic. The dispersion in the longitudinal direction of the artery could then approach the value predicted by the model ($a = 1.66$ rad). A second possible explanation is that there are additional mechanical effects at work, not accounted for by the present model. For example, Herrera et al. (2005) suggested that the overlap between myosin and actin filaments in smooth muscle varies with muscle length, and that this effect would give rise to the optimal length phenomenon observed in smooth muscle. Thus, at the higher stretch ($\lambda_3 = 1.67$), the overlap in the contractile filaments would be greater, resulting in a higher force-generating capacity. This overlap effect has been addressed in a recent study by the present author (Kroon, 2010b), where it was demonstrated that the optimal length characteristics of smooth muscle to a large extent can be explained by a variation in the overlap between actin and myosin filaments.

In general, an isotropic neoHookean model is too simplistic to fully characterise the passive behaviour of smooth muscle tissue, since the tissue is expected to be stiffer in the circumferential direction due to the preferred directions of elastin and collagen fibres. However, the experimental results at hand do not allow for assessment of a more advanced model for the pas-

sive behaviour. More importantly, in the present paper focus is on the active part of the model, and the main purpose is to demonstrate the possible influence of dispersion in contractile unit orientation on muscle behaviour. The use of a more advanced model for the passive behaviour will not affect the conclusions drawn here for the active behaviour.

The data used for evaluating the present model has relatively low complexity (two isometric tests at different stretches), and in the stress vs. time response, there are discrepancies between the model and the experiments, especially during the transients. Hence, it is mainly the steady-state stress that is being used to assess the influence of myosin filament dispersion.

During the last decade, it has also been recognised that above all airway smooth muscle is able to remodel its internal structure of the contractile apparatus and cytoskeleton (Bai et al., 2004). This remodelling occurs when the muscle is exposed to changes in length over extended periods of time. A few attempts have also been made to model this conjectured remodelling and associated time-dependent mechanical response (Lambert et al., 2004; Silveira et al., 2005; Silveira and Fredberg, 2005; Silveira et al., 2009). The immediate contractile behaviour of the muscle is, however, governed by the present internal structure of contractile units.

In summary, a new constitutive model for the biomechanical behaviour of smooth muscle tissue has been proposed, where the statistical dispersion of myosin filaments in the muscle cells is taken into account. The active muscle contraction is accomplished by the relative sliding between actin and myosin filaments, comprising contractile units in the smooth muscle cells. A strain-energy function is used to describe the mechanical behaviour of the

smooth muscle tissue. The constitutive model was compared to experiments on smooth muscle tissue from swine carotid artery, both in terms of histological data and isometric tensile test results. The model was fully able to reproduce both the histological and tensile test results well. However, the filament dispersion obtained from the histological data severely underestimated the steady-state stress in the isometric tensile tests. Two reasons for this discrepancy were offered: the myosin filament dispersion may not be perfectly axisymmetric (as was assumed in the present analysis), and there may be additional mechanical processes involved, such as a varying overlap between myosin and actin filaments.

References

Alastrue, V., Martinez, M. A., Doblare, M., Menzel, A., 2009. Anisotropic micro-sphere-based finite elasticity applied to blood vessel modelling. J. Mech. Phys. Solids 57, 178–203.

Arner, A., 1982. Mechanical characteristics of chemically skinned guinea-pig taenia coli. Pflügers Arch. – Eur. J. Physiol. 395, 277–284.

Bai, T. R., Bates, J. H. T., Brusasco, V., Camoretti-Mercado, B., Chitano, P., Deng, L. H., Dowell, M., Fabry, B., Ford, L. E., Fredberg, J. J., Gerthoffer, W. T., Gilbert, S. H., Gunst, S. J., Hai, C.-M., Halayko, A. J., Hirst, S. J., James, A. L., Janssen, L. J., Jones, K. A., King, G. G., Lakser, O. J., Lambert, R. K., Lauzon, A.-M., Lutchen, K. R., Maksym, G. N., Meiss, R. A., Mijailovich, S. M., Mitchell, H. W., Mitchell, R. W., Mitzner, W., Murphy, T. M., Pare, P. D., Schellenberg, R. R., Seow, C. Y., Sieck,

G. C., Smith, P. G., Smolensky, A. V., Solway, J., Stephens, N. L., Stewart, A. G., Tang, D. D., , Wang, L., 2004. On the terminology for describing the length-force relationship and its changes in airway smooth muscle. J. Appl. Physiol. 97, 2029–2034.

Bazant, Z. P., Oh, B. H., 1986. Efficient numerical integration on the surface of a sphere. Z. Angew. Math. Mech. 66, 37–49.

Bitar, K. N., 2003. Function of gastrointestinal smooth muscle: From signaling to contractile proteins. Am. J. Med. 115, 15S–23S.

Brophy, C. M., 2000. The dynamic regulation of blood vessel caliber. J. Vasc. Surg. 31, 391–395.

Fay, F. S., Delise, C. M., 1973. Contraction of isolated smooth muscle cells - structural changes. Proc. Natl. Acad. Sci. USA 70, 641–645.

Fung, Y. C., 1993. Biomechanics. Mechanical Properties of Living Tissues, 2nd Edition. Springer-Verlag, New York.

Gestrelius, S., Borgström, P., 1986. A dynamic model of smooth muscle contraction. Biophys. J. 50, 157–169.

Hai, C. M., Kim, H. R., 2005. An expanded latch-bridge model of protein kinase C-mediated smooth muscle contraction. J. Appl. Physiol. 98, 1356–1365.

Hai, C. M., Murphy, R. A., 1988. Cross-bridge phosphorylation and regulation of latch state in smooth muscle. Am. J. Physiol. 254, C99–C106.

Hai, C. M., Murphy, R. A., 1989. Cross-bridge dephosphorylation and relaxation of vascular smooth muscle. Am. J. Physiol. 256, C282–C287.

Herrera, A. M., McParland, B. E., Bienkowska, A., Tait, R., Par, P. D., 2005. 'Sarcomeres' of smooth muscle: functional characteristics and ultrastructural evidence. J. Cell Sci. 118, 2381–2392.

Hill, A. V., 1938. The heat of shortening and the dynamic constants of muscle. Proc. R. Soc. Lond. B 126, 136–195.

Hodgkinson, J. L., Newman, T. M., Marston, S. B., Severs, N. J., 1995. The structure of the contractile apparatus in ultrarapidly frozen smooth muscle: Freeze-fracture, deep-etch, and freeze-substitution studies. J. Struct. Biol. 114, 93–104.

Holzapfel, G. A., 2000. Nonlinear Solid Mechanics. A Continuum Approach for Engineering. John Wiley & Sons, Chichester.

Huxley, A. F., 1957. Muscle structure and theories of contraction. Prog. Biophys. and Biophys. Chem. 7, 255–318.

Huxley, A. F., Niedergerke, R., 1954. Interference microscopy of living muscle fibres. Nature 173, 971–973.

Huxley, H. E., 1953. Electron microscope studies on the organisation of the filaments in striated muscle. Biochem. Biophys. Acta. 12, 387–394.

Huxley, H. E., Hanson, J., 1954. Changes in the cross-striations of muscle during contraction and stretch and their structural interpretation. Nature 173, 973–976.

Jiang, M. J., Morgan, K. G., 1989. Agonist-specific myosin phosphorylation and intracellular calcium during isometric contractions of arterial smooth muscle. Pflügers Arch. – Eur. J. Physiol. 413, 637–643.

Kamm, K. E., Gerthoffer, W. T., Murphy, R. A., Bohr, D. F., 1989. Mechanical properties of carotid arteries from doca hypertensive swine. Hypertension 13, 102–109.

Kroon, M., 2010a. A constitutive model for smooth muscle including active tone and passive viscoelastic behaviour. Math. Med. Biol. 27, 129–155.

Kroon, M., 2010b. Optimal length of smooth muscle assessed by a microstructurally and statistically based constitutive model. Comput. Meth. Biomech. Biomed. Eng.In press.

Kuo, K. H., Seow, C. Y., 2004. Contractile filament architecture and force transmission in swine airway smooth muscle. J. Cell Sci. 117, 1503–1511.

Lambert, R. K., Pare, P. D., Seow, C. Y., 2004. Mathematical description of geometric and kinematic aspects of smooth muscle plasticity and some related morphometrics. J. Appl. Physiol. 96, 469–476.

Lee, S., Schmid-Schönbein, G. W., 1996a. Biomechanical model for the myogenic response in the microcirculation: Part I – formulation and initial testing. J. Biomech. Eng. 118, 145–151.

Lee, S., Schmid-Schönbein, G. W., 1996b. Biomechanical model for the myogenic response in the microcirculation: Part II – experimental evaluation in rat cremaster muscle. J. Biomech. Eng. 118, 152–157.

Löfgren, M., Malmqvist, U., Arner, A., 2001. Substrate and product dependence of force and shortening in fast and slow smooth muscle. J. Gen. Physiol. 117, 407–417.

Makujina, S. R., Abebe, W., Ali, S., Mustafa, S. J., 1995. Simultaneous measurement of intracellular calcium and tension in vascular smooth muscle: Validation of the everted ring preparation. J. Pharm. Toxicol. Meth 34, 157–163.

McIntyre Jr., R. C., Agrafojo, J., Banerjee, A., 1996. Pulmonary vascular smooth muscle contraction. J. Surg. Res. 61, 170–174.

Miehe, C., Göktepe, S., Lulei, F., 2004. A micro-macro approach to rubber-like materials–part i: the non-affine micro-sphere model of rubber elasticity. J. Mech. Phys. Solids 52, 2617–2660.

Miftakhov, R. N., Abdusheva, G. R., 1996. Numerical simulation of excitation-contraction coupling in a locus of the small bowel. Biol. Cybern. 74, 455–467.

Morgan, K. G., Papageorgiou, P., Jiang, M. J., 1989. Pathophysiologic role of calcium in the development of vascular smooth muscle tone. Am. J. Cardiol. 64, 35F–40F.

Murtada, S., Kroon, M., Holzapfel, G. A., 2010a. A calcium-driven mechanochemical model for prediction of force generation in smooth muscle. Biomech. Model. Mechanobio.In press.

Murtada, S., Kroon, M., Holzapfel, G. A., 2010b. Modeling the dispersion

effects of contractile fibers in smooth muscles. J. Mech. Phys. SolidsIn press.

Paul, R. J., 1990. Smooth muscle energetics and theories of cross-bridge regulation. Am. J. Physiol. 258, C369–C375.

Peterson, J. W., 1982. Simple model of smooth muscle myosin phosphorylation and dephosphorylation as rate-limiting mechanism. Biophys. J. 37, 453–459.

Rachev, A., Hayashi, K., 1999. Theoretical study of the effects of vascular smooth muscle contraction on strain and stress distributions in arteries. Ann. Biomed. Eng. 27, 459–468.

Rembold, C. M., Murphy, R. A., 1990a. Latch-bridge model in smooth muscle: $[Ca^{2+}]$ can quantitatively predict stress. Am. J. Physiol. 259, C251–C257.

Rembold, C. M., Murphy, R. A., 1990b. Muscle length, shortening, myoplasmic $[Ca^{2+}]$, and activation of arterial smooth muscle. Circ. Res. 66, 1354–1361.

Rosenbluth, J., 1965. Smooth muscle: an ultrastructural basis for the dynamics of its contraction. Science 148, 1337–1339.

Roy, S., Silacci, P., Stergiopulos, N., 2005. Biomechanical properties of decellularized porcine common carotid arteries. Am. J. Physiol. Heart Circ. Physiol. 289, 1567–1576.

Seow, C. Y., Par, P. D., 2007. Ultrastructural basis of airway smooth muscle contraction. Can. J. Physiol. Pharmacol. 85, 659–665.

Silveira, P. S. P., Alencar, A. M., Majumdar, A., Lemos, M., Fredberg, J. J., Suki, B., 2009. Percolation in a network with long-range connections: Implications for cytoskeletal structure and function. Phys. A 388, 1521–1526.

Silveira, P. S. P., Butler, J. P., Fredberg, J. J., 2005. Length adaptation of airway smooth muscle: a stochastic model of cytoskeletal dynamics. J. Appl. Physiol. 99, 2087–2098.

Silveira, P. S. P., Fredberg, J. J., 2005. Smooth muscle length adaptation and actin filament length: a network model of the cytoskeletal dysregulation. Can. J. Physiol. Pharmacol. 83, 923–931.

Silver, F. H., Snowhill, P. B., Foran, D. J., 2003. Mechanical behavior of vessel wall: A comparative study of aorta, vena cava, and carotid artery. Ann. Biomed. Eng. 31, 793–803.

Stålhand, J., Klarbring, A., Holzapfel, G. A., 2008. Smooth muscle contraction: mechanochemical formulation for homogeneous finite strains. Prog. Biophys. Molec. Biol. 96, 465–481.

Takamizawa, K., Hayashi, K., 1987. Strain energy density function and uniform strain hypothesis for arterial mechanics. J. Biomech. 20, 7–17.

Tang, D. C., Stull, J. T., Kubota, Y., Kamm, K. E., 1992. Regulation of the [Ca^{2+}] dependence of smooth muscle contraction. J. Bio. Chem. 267, 11839–11845.

Tosun, M., Paul, R. J., Rapoport, R. M., 1997. Intracellular [Ca^{2+}] elevation and contraction due to prostaglandin f2alpha in rat aorta. Eur. J. Pharmacol. 340, 203–208.

Walker, J. S., Wingard, C. J., Murphy, R. A., 1994. Energetics of crossbridge phosphorylation and contraction in vascular smooth muscle. Hypertension 23, 1106–1112.

Walmsley, J. G., Murphy, R. A., 1987. Force-length dependence of arterial lamellar, smooth muscle, and myofilament orientations. Am. J. Physiol. Heart Circ. Physiol. 253, H1141–H1147.

Yang, J., Clark Jr., J. W., Bryan, R. M., Robertson, C., 2003a. The myogenic response in isolated rat cerebrovascular arteries: smooth muscle cell model. Medical Engineering & Physics 25, 691–709.

Yang, J., Clark Jr., J. W., Bryan, R. M., Robertson, C., 2003b. The myogenic response in isolated rat cerebrovascular arteries: vessel model. Medical Engineering & Physics 25, 711–717.

Zulliger, M. A., Rachev, A., Stergiopulos, N., 2004. A constitutive formulation of arterial mechanics including vascular smooth muscle tone. Am. J. Physiol. Heart Circ. Physiol. 287, H1335–H1343.